

Tracking QCD–Instantons

F. Schrempf

Deutsches Elektronen-Synchrotron DESY, Hamburg, Germany

Abstract. In a first part, I review our detailed investigation of the prospects to discover deep-inelastic processes induced by small QCD-instantons at HERA. This includes the essence of our calculations based on instanton-perturbation theory, crucial lattice constraints and a confrontation of the recent intriguing (preliminary) search results by the H1 collaboration with our predictions. In a second part, I report on two ongoing attempts towards a better understanding of the rôle of larger-size instantons in the QCD-vacuum and in high-energy (diffractive) scattering processes, respectively: The striking suppression of larger-size instantons in the vacuum is attributed to a residual conformal inversion symmetry, and a precocious lack of “color transparency” in the one-instanton contribution to the color-dipole scattering picture is emphasized.

1. Introduction

Instantons[1, 2] represent a basic non-perturbative aspect of QCD, but their direct experimental verification is still lacking. Being topologically non-trivial fluctuations of the gluon fields, QCD-instantons induce hard, chirality-violating processes absent in conventional perturbation theory[2]. Deep-inelastic scattering (DIS) at HERA has been shown to offer a unique opportunity[3] to discover such processes induced by *small* instantons (I) through a sizable[†] rate[5, 6, 7] and a characteristic final-state signature [3, 8, 9, 10]. A first part of this talk is devoted to a review of our extensive investigation on small instantons in deep-inelastic scattering. This includes a “flow-chart” of our calculations based on I -perturbation theory[5, 6], an exploitation of crucial lattice constraints[7, 11] and a confrontation[10] of the recent intriguing (preliminary) I -search results by the H1 collaboration[12, 13, 14] with our predictions. In a second part, I report on two ongoing attempts[15, 16] towards a better understanding of the rôle of *larger-size* instantons in the QCD-vacuum and in high-energy (diffractive) scattering processes, respectively: The striking suppression of larger-size instantons in the vacuum is attributed to a residual *conformal inversion* symmetry[15], and an interesting, precocious lack of “color transparency” in the one-instanton contribution[16] to the color-dipole scattering picture[17] in the deep-inelastic regime is emphasized.

[†] For an exploratory calculation of the instanton contribution to the gluon-structure function, see Ref. [4].

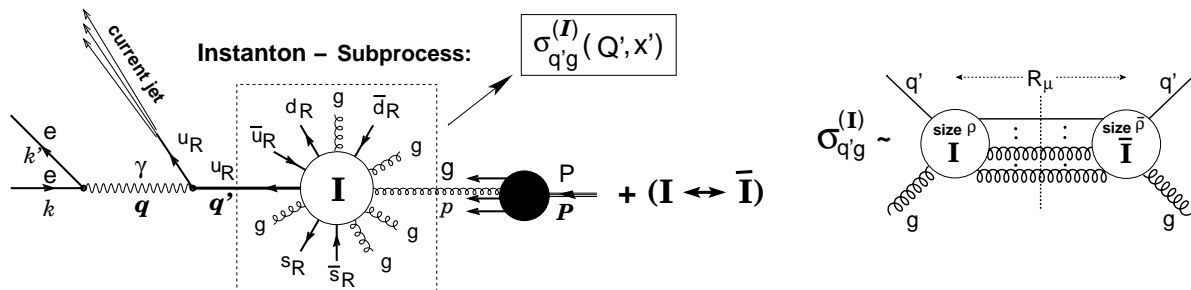


Figure 1. (left): Leading, instanton-induced process in deep-inelastic $e^\pm P$ scattering for $n_f = 3$. (right): Structure of the total cross section for the chirality-violating “instanton-subprocess” $q'g \Rightarrow X$ and illustration of the collective coordinates $\rho, \bar{\rho}, R_\mu$.

2. Small instantons and deep-inelastic scattering

2.1. Instanton-perturbation theory

Let us start by briefly summarizing the essence of our theoretical calculations[5, 6] based on so-called I -perturbation theory. As we shall see below, in an appropriate phase-space region of deep-inelastic scattering with generic hard scale Q , the contributing I 's and \bar{I} 's have *small size* $\rho \lesssim \mathcal{O}(\frac{1}{\alpha_s(Q)Q})$ and may be self-consistently considered as a *dilute* gas, with the small QCD coupling $\alpha_s(Q)$ being the expansion parameter like in usual perturbative QCD (pQCD). Unlike the familiar expansion about the trivial vacuum $A_\mu^{(0)} = 0$ in pQCD, in I -perturbation theory the path integral for the generating functional of the Green's functions in Euclidean position space is then expanded about the known, classical one-instanton solution, $A_\mu = A_\mu^{(I)}(x) + \dots$. After Fourier transformation to momentum space, LSZ amputation and careful analytic continuation to Minkowski space (where the actual on-shell limits are taken), one obtains a corresponding set of modified Feynman rules for calculating I -induced scattering amplitudes. As a further prerequisite, the masses m_q of the active quark flavours must be light on the scale of the inverse effective I -size $1/\rho_{\text{eff}}$, i. e. $m_q \cdot \rho_{\text{eff}} \ll 1$.

The leading, I -induced, chirality-violating process in the deep-inelastic regime of $e^\pm P$ scattering is displayed in Figure 1 (left) for $n_f = 3$ massless flavors. In the background of an I (\bar{I}) (of topological charge $Q = +1$ (-1)), all n_f massless quarks and anti-quarks are right (left)-handed such that the I -induced subprocess emphasized in Figure 1 (left) involves a violation of chirality $Q_5 = \#(q_R + \bar{q}_R) - \#(q_L + \bar{q}_L)$ by an amount,

$$\Delta Q_5 = 2 n_f Q, \quad (1)$$

in accord with the general chiral anomaly relation[2]. Within I -perturbation theory, one first of all derives the following factorized expression in the Bjorken limit of the I -subprocess variables Q'^2 and x' (c.f. Figure 1 (left)):

$$\frac{d\sigma_{\text{HERA}}^{(I)}}{dx'dQ'^2} \simeq \frac{d\mathcal{L}_{q'g}^{(I)}}{dx'dQ'^2} \cdot \sigma_{q'g}^{(I)}(Q', x') \quad \text{for} \quad \begin{cases} Q'^2 = -q'^2 > 0 \text{ large,} \\ 0 \leq x' = \frac{Q'^2}{2p \cdot q'} \leq 1 \text{ fixed.} \end{cases} \quad (2)$$

In Equation (2), the differential luminosity, $d\mathcal{L}_{q'g}^{(I)}$ counts the number of $q'g$ collisions per eP collisions. It is given in terms of integrals over the gluon density, the virtual photon flux, and the (known) flux of the virtual quark q' in the instanton background[6].

The essential instanton dynamics resides, however, in the total cross-section of the I -subprocess $q'g \xrightarrow{I} X$ as emphasized in Figure 1. Being an observable, $\sigma_{q'g}^{(I)}(Q', x')$ involves integrations over all I and \bar{I} -“collective coordinates”, i. e. the I (\bar{I}) sizes ρ ($\bar{\rho}$), the $I\bar{I}$ distance four-vector R_μ and the relative $I\bar{I}$ color orientation matrix U .

$$\sigma_{q'g}^{(I)} = \int d^4R e^{i(p+q')\cdot R} \int_0^\infty d\rho \int_0^\infty d\bar{\rho} e^{-(\rho+\bar{\rho})Q'} D(\rho) D(\bar{\rho}) \int dU e^{-\frac{4\pi}{\alpha_s} \Omega\left(U, \frac{R^2}{\rho\bar{\rho}}, \frac{\bar{\rho}}{\rho}\right)} \{...\} \quad (3)$$

Both instanton and anti-instanton degrees of freedom enter here, since cross-sections result from taking the modulus squared of an amplitude in the single I -background. Alternatively and more conveniently (c. f. Figure 1 (right)), one may obtain the cross-section (3) as a discontinuity of the $q'g$ forward elastic scattering amplitude in the $I\bar{I}$ -background [6]. The $\{...\}$ in Equation (3) abbreviates smooth contributions associated with the external partons etc.

Let us concentrate on two crucial and strongly varying quantities of the I -calculus appearing in Equation (3): $D(\rho)$, the (reduced) I -size distribution[2, 18], and $\Omega\left(U, \frac{R^2}{\rho\bar{\rho}}, \frac{\bar{\rho}}{\rho}\right)$, the $I\bar{I}$ interaction[19, 20], associated with a resummation of final-state gluons. Both objects are *known* within I -perturbation theory, formally for $\alpha_s(\mu_r) \ln(\mu_r \rho) \ll 1$ and $\frac{R^2}{\rho\bar{\rho}} \gg 1$ (diluteness), respectively, with μ_r being the renormalization scale.

Most importantly, the resulting power-law behaviour for the I -size distribution,

$$D(\rho) \propto \rho^{\beta_0 - 5 + \mathcal{O}(\alpha_s)}, \quad (4)$$

involving the leading QCD β -function coefficient, $\beta_0 = \frac{11}{3} N_c - \frac{2}{3} n_f$, ($N_c = 3$), generically spoils the calculability of I -observables due to the bad IR-divergence of the integrations over the I (\bar{I})-sizes for large ρ ($\bar{\rho}$). Deep-inelastic scattering represents, however, a crucial exception: The *exponential* “form factor” $\exp(-Q'(\rho + \bar{\rho}))$ that was shown[5] to arise in Equation (3), insures convergence and *small* instantons for large enough Q' , despite the strong power-law growth of $D(\rho)$. This is the key feature, warranting the calculability of I -predictions for DIS.

It turns out that for (large) $Q' \neq 0$, all collective coordinate integrations in $\sigma_{q'g}^{(I)}$ of Equation (3) may be performed in terms of a *unique saddle point*:

$$U^* \Leftrightarrow \text{most attractive relative } I\bar{I} \text{ orientation in color space,} \\ \rho^* = \bar{\rho}^* \sim \frac{4\pi}{\alpha_s(\frac{1}{\rho^*})} \frac{1}{Q'}; \quad \frac{R^{*2}}{\rho^{*2}} \underset{Q' \text{ large}}{\sim} 4 \frac{x'}{1-x'} \quad (5)$$

This result underlines the self-consistency of the approach, since for large Q' and small $(1-x')$ the saddle point (5), indeed, corresponds to widely separated, small I 's and \bar{I} 's.

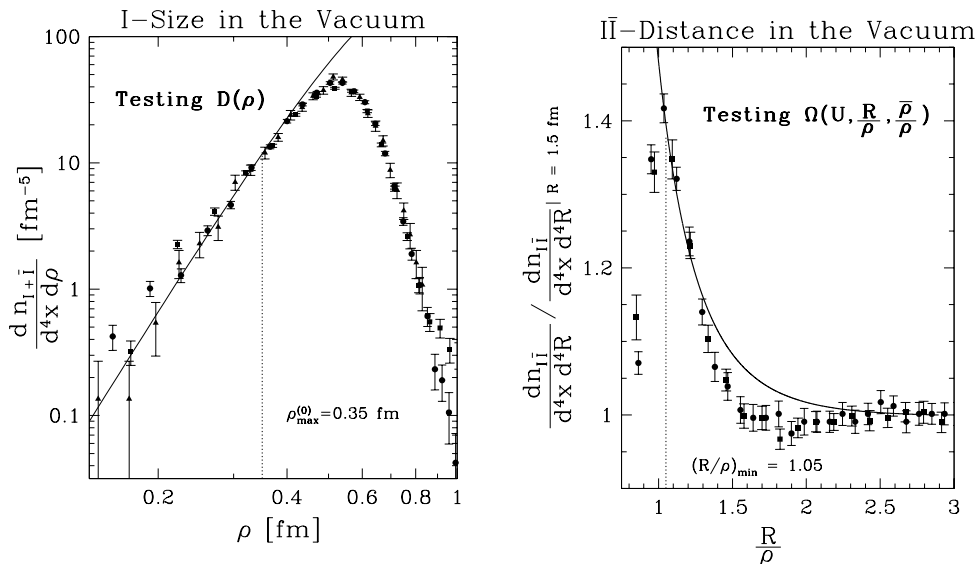


Figure 2. Illustration of the agreement of recent high-quality lattice data [11, 7] for the instanton-size distribution (left) and the normalized $I\bar{I}$ -distance distribution (right) with the predictions from instanton-perturbation theory [7] for $\rho \lesssim 0.35$ fm and $R/\rho \gtrsim 1.05$, respectively. $\alpha_{\overline{\text{MS}}}^{3\text{-loop}}$ with $\Lambda_{\overline{\text{MS}}}^{(n_f=0)}$ from ALPHA [21] was used.

2.2. Region of validity of the predictions

The I -size distribution $D(\rho)$ and the $I\bar{I}$ interaction $\Omega\left(U, \frac{R^2}{\rho\bar{\rho}}, \frac{\bar{\rho}}{\rho}\right)$ form a crucial link between deep-inelastic scattering and lattice observables in QCD vacuum[7].

Lattice simulations, on the other hand, provide independent, non-perturbative information on the *actual* range of validity of the form predicted from I -perturbation theory for these important functions of ρ and R/ρ , respectively. The one-to-one saddle-point correspondence (5) of the (effective) collective I -coordinates $(\rho^*, R^*/\rho^*)$ to (Q', x') may then be exploited to arrive at a “fiducial” (Q', x') region for our predictions in DIS. Let us briefly summarize the results of this strategy[7].

We have used the recent high-quality lattice data[11, 7] for quenched QCD ($n_f = 0$) by the UKQCD collaboration together with the careful, non-perturbative lattice determination of the respective QCD Λ -parameter, $\Lambda_{\overline{\text{MS}}}^{(n_f=0)} = (238 \pm 19)$ MeV, by the ALPHA collaboration[21]. The results of an essentially parameter-free comparison of the continuum limit[7] for the simulated $(I + \bar{I})$ -size and the $I\bar{I}$ -distance distributions with I -perturbation theory versus ρ and R/ρ , respectively, is displayed in Figure 2. The UKQCD data for the $I\bar{I}$ -distance distribution provide the first direct test of the $I\bar{I}$ interaction $\Omega\left(U, \frac{R^2}{\rho\bar{\rho}}, \frac{\bar{\rho}}{\rho}\right)$ via[7]

$$\frac{d n_{I\bar{I}}}{d^4 x d^4 R}|_{\text{UKQCD}} \stackrel{?}{\simeq} \int_0^\infty d\rho \int_0^\infty d\bar{\rho} D(\rho) D(\bar{\rho}) \int dU e^{-\frac{4\pi}{\alpha_s} \Omega\left(U, \frac{R^2}{\rho\bar{\rho}}, \frac{\bar{\rho}}{\rho}\right)}, \quad (6)$$

and the lattice measurements of $D(\rho)$.

From Figure 2, I -perturbation theory appears to be quantitatively valid for

$$\left. \begin{array}{l} \rho \cdot \Lambda_{\overline{\text{MS}}}^{(n_f=0)} \gtrsim 0.42 \\ R/\rho \gtrsim 1.05 \end{array} \right\} \text{saddle point} \Rightarrow \left\{ \begin{array}{l} Q'/\Lambda_{\overline{\text{MS}}}^{(n_f)} \gtrsim 30.8, \\ x' \gtrsim 0.35, \end{array} \right. \quad (7)$$

Beyond providing a quantitative estimate for the “fiducial” momentum space region in DIS, the good, parameter-free agreement of the lattice data with I -perturbation theory is very interesting in its own right. Uncertainties associated with the inequalities (7) are studied in detail in Ref. [10].

2.3. Characteristic final-state signature

The qualitative origin of the characteristic final-state signature of I -induced events is intuitively explained and illustrated in Figure 3. An indispensable tool for a quantitative investigation of the characteristic final-state signature and notably for actual experimental searches of I -induced events at HERA is our Monte-Carlo generator package QCDINS[9].

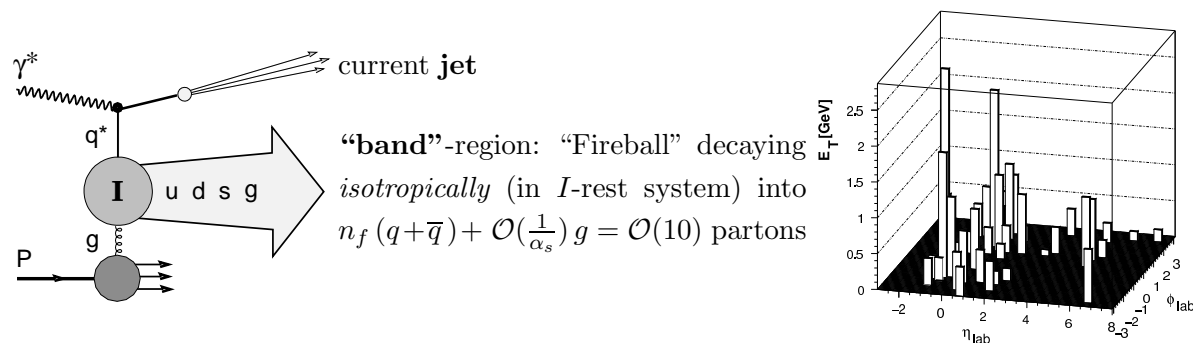


Figure 3. Characteristic signature of I -induced events: *One* (current) *jet* along with a densely filled *band* of hadrons in the (η, ϕ) plane. Each event has large hadron multiplicity, large total E_t , u-d-s flavor democracy with 1 $s\bar{s}$ -pair/event leading to $K's, \Lambda's \dots$. An event from our QCDINS[9] generator (right) illustrates these features.

2.4. First dedicated search results versus theory

At the recent DIS2000 and ICHEP2000 conferences, the H1 collaboration has reported preliminary results of a first dedicated search for instanton-induced events at HERA[12, 13]. The results presented are quite intriguing and encouraging, although far from being conclusive. In view of a separate experimental talk on these data at this meeting[14], let us briefly summarize and discuss these findings from a theorist’s perspective, while keeping comments on experimental aspects at a minimum.

The H1 analysis is based on the strategy[8] of isolating an “instanton-enriched” data sample by means of suitable cuts to a set of three instanton-sensitive, discriminating observables. Three different cut-scenarios A), B) and C) with *increasing* instanton-separation power $\epsilon_I/\epsilon_{\text{nDIS}}$ were considered, with ϵ_I and ϵ_{nDIS} being the efficiencies for

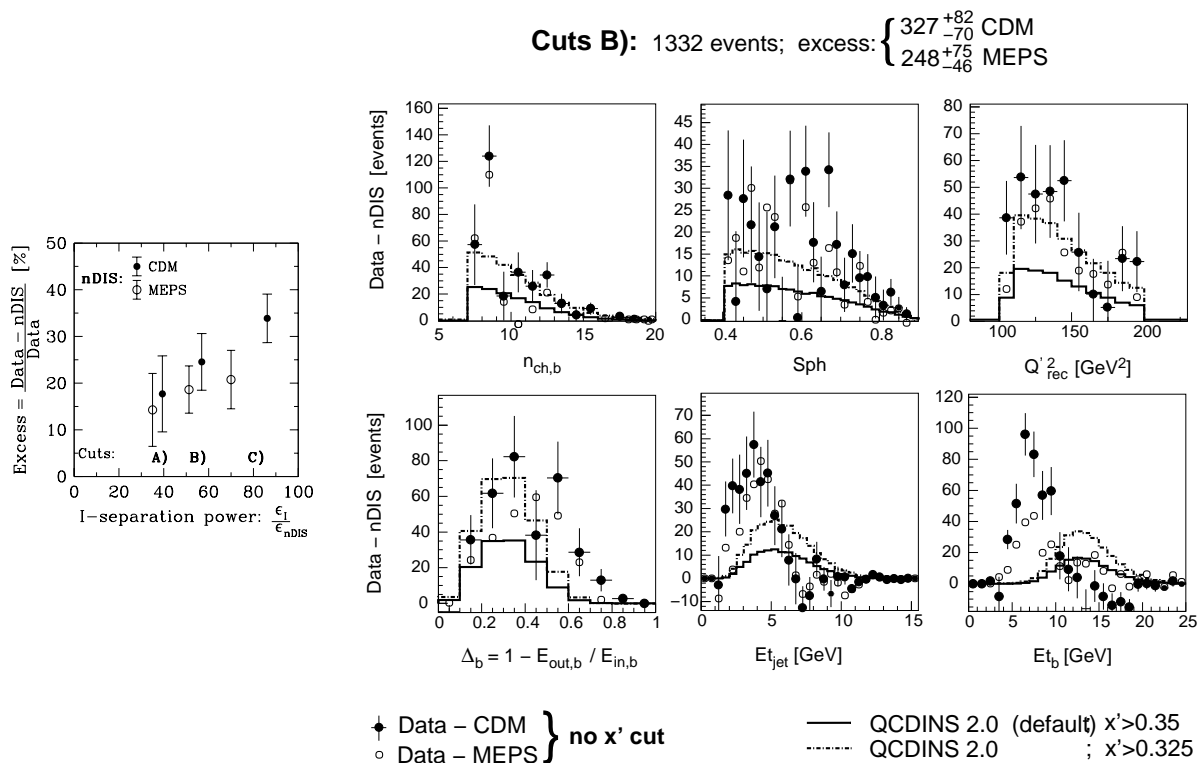


Figure 4. Summary of preliminary H1 data from a dedicated search for instanton-induced events[12, 13] along with our parameter-free predictions. (left): The observed excess over normal DIS events according to standard Monte Carlo generators[22, 23] appears to increase with the instanton-separation power. (right): Excess in the six considered observables (8, 9) compared to our predictions from QCDINS[9]. The size of the instanton-signal is fixed in terms of $\Lambda_{\overline{\text{MS}}}^{(5)} = 219$ MeV (1998 world average [24]).

I -events (QCDINS[9] generator) and normal DIS-events (two generators: CDM=“Color Dipole Model” (ARIADNE[22]) and MEPS (RAPGAP[23])), respectively.

In a phase space region, where a reduction of the normal DIS (nDIS) background to the percent level is achieved according to the considered Monte Carlo models, a (statistically) significant excess of events was found in the H1 data. Figure 4 (left), displays the experimentally observed excess versus the I -separation power, the latter being a purely theoretical quantity determined from the I - and nDIS event generators. It is quite remarkable that experiment and theory seem to be correlated, i. e. that the excess tends to increase with increasing I -separation power.

The observed excess along with our original, parameter-free theoretical predictions[6, 9] in the six considered distributions[12, 13, 14] of I -sensitive observables is displayed in Figure 4 (right). The first row shows the three discriminating observables,

$$\begin{aligned}
 n_{ch,b} &: \text{ number of charged hadrons in the } I\text{-“band” region} \\
 Sph &: \text{ sphericity in the rest system of “non-jet”-particles} \\
 Q_{\text{rec}}^{\prime 2} &: \text{ reconstructed virtuality of the } I\text{-subprocess quark } q'
 \end{aligned} \tag{8}$$

while the second row displays three further observables without additional cuts applied,

$$\begin{aligned}
 \Delta_b &: Et\text{-weighted azimuthal-isotropy} \\
 Et_{\text{jet}} &: \text{transverse energy of the current-jet} \\
 Et_b &: \text{total transverse energy in the } I\text{-"band" region.}
 \end{aligned}
 \tag{9}$$

In the first four of the six observables in Figure 4, the excess is intriguingly similar in shape and normalization to our theoretical predictions from QCDINS, although its size is partly at a level still comparable to the differences among the considered DIS event generators. While the size of the observed excess in the remaining two observables, Et_b and Et_{jet} , is in rough agreement as well, the peaks of these two experimental distributions appear to be shifted towards smaller values compared to QCDINS, and the widths are also considerably narrower.

Here, some important theoretical comments are in place[10]. One has to take into account that so far the preliminary H1 data incorporate only part of the theoretically required cuts: While the $Q'^2 \gtrsim 113 \text{ GeV}^2$ cut (7) has been applied to the data, both the x' -cut (7) and notably a further cut on Q^2 ,

$$Q^2 \gtrsim Q_{\text{min}}^2 = 113 \text{ GeV}^2, \tag{10}$$

(c.f. Refs. [5, 9]), are lacking. In Refs. [12, 13, 14], as well as in Figure 4(right) (solid line), these data are compared to the QCDINS output with *active* x' -cut (7), but with the default Q^2 -cut (10) switched off to match the data.

The implications of the lacking x' -cut in the data are presumably not too serious, since QCDINS *with* the default x' -cut models to some extent the sharp suppression of I -effects, apparent in the lattice data (c.f. Figure 2 (right)) for $R/\rho \lesssim 1.0 - 1.05$, i.e. $x' \lesssim 0.3 - 0.35$. Yet, this lacking, experimental cut introduces a substantial uncertainty in the predicted magnitude of the I -signal that hopefully may be eliminated soon. The dash-dotted line in Figure 4 (right) illustrates that the overall size of the I -signal strongly depends on the actual value of the x' -cut used in QCDINS. The slightly reduced value of $x'_{\text{min}} = 0.325$ in Figure 4(right) is certainly compatible with Figure 2 (right), but improves the agreement with the observed excess considerably, as compared to the default $x'_{\text{min}} = 0.35$.

Next, consider the effects of the lacking Q^2 -cut (10). As a brief reminder[5, 9], this cut assures in particular the dominance of “planar” handbag-type graphs in $\sigma_{\text{HERA}}^{(I)}$ and all final-state observables. The non-planar contributions do not share the simple, probabilistic interpretation of the planar ones, involve instantons with a size determined by $1/Q$ rather than $1/Q'$ and are both hard to calculate and hard to implement in a Monte Carlo generator. On account of their known power suppression in $1/Q^2$ and a cross-check in the simplest case without final-state gluons[5], they can be safely neglected upon application of the cut (10). Because of these reasons, the non-planar contributions are *not* implemented in the QCDINS event generator, corresponding to unreliable QCDINS results for small Q^2 .

From a detailed study of the effects of the lacking Q^2 -cut (10) in Ref. [10], the following conclusions have emerged.

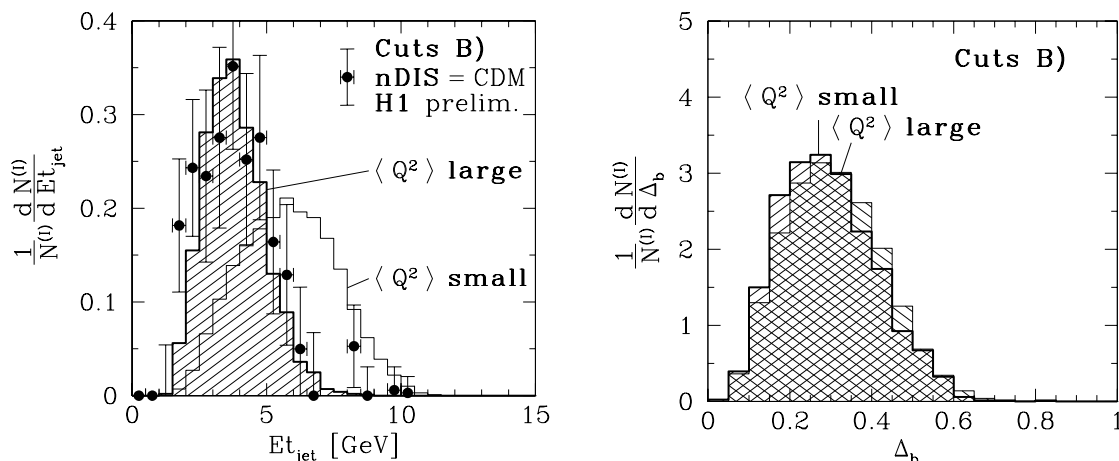


Figure 5. Effect of the lacking Q^2 -cut on the predicted excess, i. e. the I -signal. (left): The *reliable portion* of generated I -events (with high $\langle Q^2 \rangle$) is distributed in Et_{jet} (and in Et_b) quite like the measured excess (H1 preliminary[12, 13, 14]). (right): The Q^2 -cut has little effect on the *shape* of the remaining four observable distributions. All histograms are from QCDINS[9].

- The shape of the Et_{jet} and Et_b distributions for I -events are strongly affected by the missing Q^2 -cut (see e. g. Et_{jet} in Figure 5 (left)), unlike the four remaining observables (see e. g. Δ_b in Figure 5 (right)).
- By cutting out the phase space region where QCDINS is unreliable ($Q^2 \lesssim Q_{\text{min}}'^2 = 113 \text{ GeV}^2$), both the resulting Et_{jet} and Et_b -peaks are left-shifted and become narrower, in good agreement with the shape-normalized H1-excess (see e. g. Et_{jet} in Figure 5 (left)). While further reaching conclusions will require the actual implementation of the Q^2 -cut (10) in the data, this exercise shows that at least the *reliable portion* of generated I -events (with high $\langle Q^2 \rangle$) is distributed in Et_{jet} and in Et_b quite like the observed excess.

Despite an improved overall agreement and understanding via such considerations, let us close this section with a reminder of the basic remaining problematics: The observed excess is strongly relying on Monte Carlo generators for *normal* DIS events, and the I -signal is expected where the latter are not too well known/studied

3. Larger-size instantons

This section is devoted to some ongoing attempts towards a better understanding of the rôle of larger-size instantons both in the QCD-vacuum and in high-energy (diffractive) scattering processes. The guidance from recent high-quality lattice simulations is indispensable in this regime, as will become evident next.

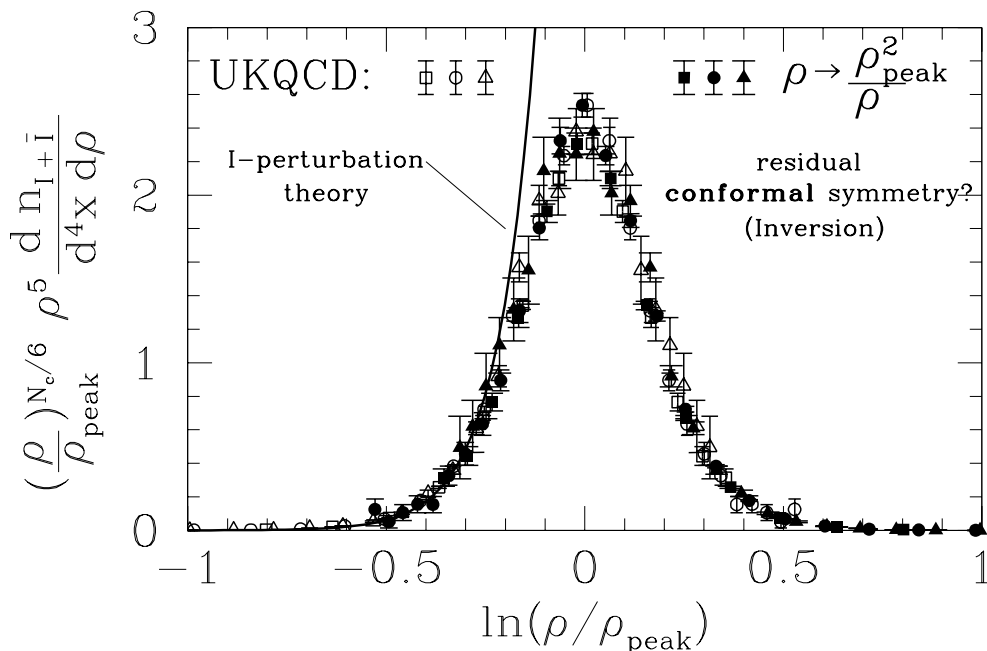


Figure 6. Same UKQCD lattice data[11, 7] for the instanton-size distribution as in Figure 2, displayed however such as to suggest a virtually perfect *inversion symmetry* under $\rho \Rightarrow \rho_{\text{peak}}^2/\rho$ with $\rho_{\text{peak}} \approx 0.6$ fm (open and solid data symbols fit onto one universal, symmetric curve). The solid line refers to instanton-perturbation theory analogous to Figure 2.

3.1. A residual conformal inversion symmetry?

Let us start by considering again the high-quality UKQCD lattice data[11, 7] for the I -size distribution $d n/d^4 x d \rho$. Unlike Figure 2(left), in Figure 6 the dimensionless quantity $(\rho/\rho_{\text{peak}})^{(N_c/6)} \rho^5 d n/d^4 x d \rho$ is now displayed versus $\ln(\rho/\rho_{\text{peak}})$, with $\rho_{\text{peak}} = 0.605$ fm being the (empirical) peak position.

The lattice data in Figure 6 first of all illustrate the striking fact that larger-size instantons are dramatically suppressed in comparison to (naive) expectations from I -perturbation theory (solid line). The peak position, ρ_{peak} , may be viewed as an important length scale, characterizing the fairly rapid breakdown of usual I -perturbation theory. It is clearly important, to ask what kind of underlying physics can give rise to such a rapid and dramatic change. The focus here will be on an intriguing, possible explanation[15] in terms of a residual conformal *inversion symmetry*.

The reason for displaying the lattice data in Figure 6 versus $\ln(\rho/\rho_{\text{peak}})$ was to make the virtually perfect

$$\text{inversion symmetry: } \rho \Leftrightarrow \frac{\rho_{\text{peak}}^2}{\rho} \quad (11)$$

self-evident in the lattice data. Both the open data symbols, referring to the original data points, and the solid ones, involving inverted arguments according to (11), seem to beautifully fit onto one universal, symmetric curve.

The possibility of such an inversion symmetry is particularly appealing, since it may well be a “relict” from the well-known *conformal invariance* of the whole I -sector at the classical level[25]. If true, such a symmetry would allow to access the non-perturbative regime of large-size instantons (yet with *small* $\rho' = \rho_{\text{peak}}^2/\rho$) in terms of I -perturbation theory for instantons with *small* ρ . It may well have also intriguing consequences beyond instanton physics for QCD in general, as we shall briefly speculate further below.

The conformal symmetry group comprises‡ besides the inhomogeneous Lorentz group (Poincaré invariance), scale transformations, $x'_\mu \Rightarrow x_\mu/\lambda$, and the coordinate *inversion*:

$$x_\mu \Rightarrow x'_\mu = \frac{\rho_0^2}{x^2} x_\mu. \quad (12)$$

The invariance under scale transformations is well-known to be broken at the quantum level via regularization/renormalization. A detailed and notably more rigorous discussion about the validity of the conformal inversion at the quantum level (I -size distribution!), would certainly lead beyond the scope of this talk and may be found elsewhere[15]. Yet, it may be instructive to sketch a few simple arguments from Ref. [15]. First of all, let us ask at the classical level, why a coordinate inversion (12) indeed implies an inversion (11) of the instanton size. For simplicity, let us consider a pure SU(2) Yang-Mills theory (no fermions). Starting from the familiar expression for the vector potential of an instanton in singular gauge (gauge coupling g),

$$A_\mu^{(I)a}(x; \rho) = \frac{2}{g} \frac{\rho^2}{x^2} \frac{\bar{\eta}_{a\mu\nu} x^\nu}{x^2 + \rho^2}, \quad (13)$$

involving the 't Hooft coefficients[2] $\bar{\eta}_{a\mu\nu}$, one straightforwardly finds for the transformed vector field $A'_\mu^{(I)a}(x; \rho)$ after a conformal coordinate inversion (12),

$$A_\mu^{(I)a}(x; \rho) \Rightarrow A'_\mu^{(I)a}(x; \rho) = A_\nu^{(I)a}(x'; \rho) \frac{dx'^\nu}{dx^\mu} = A_\mu^{(\bar{I})a}(x; \frac{\rho_0^2}{\rho})|_{\text{regular gauge}}. \quad (14)$$

Apparently, the inversion (12) transforms the vector potential in singular gauge of an instanton with size ρ into the vector potential in regular gauge of an *anti*-instanton with size ρ_0^2/ρ ! Using the conformal transformation law of the field-strength tensor,

$$G_{\mu\nu}^a(x) \Rightarrow G'_{\mu\nu}{}^a(x) = G_{\alpha\beta}^a(x') \frac{dx'^\alpha}{dx^\mu} \frac{dx'^\beta}{dx^\nu}, \quad (15)$$

one arrives after some calculation at the following (gauge-independent) transformation of the (anti-) instanton contribution to the Lagrange density,

$$\mathcal{L}^{(I)}(x, \rho) = \frac{1}{4} G_{\mu\nu}^{(I)a}(x, \rho) G^{(I)a\mu\nu}(x, \rho) \Rightarrow \mathcal{L}'^{(I)}(x, \rho) = \mathcal{L}^{(I)}(x, \frac{\rho_0^2}{\rho}), \quad (16)$$

which illustrates the I -size inversion (11) of interest as resulting from the coordinate inversion (12). Upon integration over space-time one then explicitly checks the

‡ In Euclidean space, the analog of Poincaré invariance is Euclidean invariance. Note moreover, that the inversion is not continuously connected to the identity. In order to discuss conformal transformations infinitesimally, one usually considers instead the so-called special conformal transformations that involve an inversion followed by a translation and another inversion.

invariance of the I -action $S^{(I)}$ under coordinate inversion due to its independence of the I -size,

$$S^{(I)} \equiv \int d^4x \mathcal{L}^{(I)}(x, \rho) = \int d^4x \mathcal{L}^{(I)}(x, \frac{\rho_0^2}{\rho}) = \int d^4x \mathcal{L}'^{(I)}(x, \rho) = \frac{8\pi^2}{g^2}. \quad (17)$$

The essential step, however, is to reconsider[15] the derivation of the (1-loop) vacuum-to-vacuum (tunnelling) amplitude[2, 18] about a single instanton that directly determines the leading expression for the I -size distribution. The task is to compare the result for instantons with *small* ρ to that for instantons with *small* $\rho' = \rho_{\text{peak}}^2/\rho$. It turns out that the (dominating) *zero-mode* contribution indeed respects the inversion symmetry (11), while a non-invariant piece due to the various non-zero mode determinants has been studied long ago[27], may be isolated and then divided out in form of the factor $(\rho/\rho_{\text{peak}})^{(N_c/6)}$ in Figure 6.

An important challenge in this approach relies in a better understanding of the significance of the inversion scale ρ_{peak} . While unbroken scale invariance would (nonsensically) make *any value* of ρ_{peak} physically equivalent, its breaking signalled by the non-vanishing trace of the energy-momentum tensor[26], $\theta_\mu^\mu \propto -\langle 0 | \frac{\alpha_s}{\pi} G_{\mu\nu}^a{}^2 | 0 \rangle$, suggests $\rho_{\text{peak}} \sim \langle 0 | \frac{\alpha_s}{\pi} G_{\mu\nu}^a{}^2 | 0 \rangle^{-1/4}$.

Let us close with pointing out an intriguing possible consequence of such an inversion symmetry of the I -size distribution, that affects α_s and thus QCD in general. Let us follow Ref.[7] and define a (non-perturbative) “ I -scheme” for $\alpha_s(\mu_r)$, after identifying the renormalization scale μ_r as $\mu_r = \frac{s_I}{\rho}$ with $s_I = \mathcal{O}(1)$, by the requirement that the familiar perturbative expression of $\rho^5 \frac{d n_I}{d^4x d\rho} [\alpha_s, s_I]$ be valid for all $\alpha_s(\frac{s_I}{\rho})$. Surprisingly, the form of $\alpha_s(\frac{s_I}{\rho})$, implicitly defined by this prescription and directly extracted from a comparison with the UKQCD data[11, 7], showed a Cornell form $\alpha_s \approx \frac{3}{4} \sigma \rho^2 + \dots$ for $\rho \gtrsim \rho_{\text{peak}}$ with string tension $\sqrt{\sigma} \approx 472$ MeV, while beautifully agreeing with the 3-loop perturbative form of $\alpha_{\overline{\text{MS}}}$ for $\rho \lesssim \rho_{\text{peak}}$. Taking here for the sake of simplicity the leading 1-loop expression for the I -size distribution[2, 18], the inversion symmetry (11) of the quantity in Figure 6 implies

$$\begin{aligned} \left(\frac{\rho}{\rho_{\text{peak}}} \right)^{(N_c/6)} \rho^5 \frac{d n_I}{d^4x d\rho} &\equiv \text{const.} \left(\frac{\rho}{\rho_{\text{peak}}} \right)^{(N_c/6)} \left(\frac{2\pi}{\alpha_s(\frac{s_I}{\rho})} \right)^{2N_c} \exp\left(-\frac{2\pi}{\alpha_s(\frac{s_I}{\rho})}\right) \\ &= \text{const.} \left(\frac{\rho_{\text{peak}}}{\rho} \right)^{(N_c/6)} \left(\frac{2\pi}{\alpha_s(\frac{s_I \rho}{\rho_{\text{peak}}^2})} \right)^{2N_c} \exp\left(-\frac{2\pi}{\alpha_s(\frac{s_I \rho}{\rho_{\text{peak}}^2})}\right). \end{aligned} \quad (18)$$

We may explicitly solve Equation (18) for $\alpha_s(\frac{s_I}{\rho})$ in terms of $\alpha_s(\frac{s_I \rho}{\rho_{\text{peak}}^2})$, which involves the Lambert-W function, $W(x) \exp(W(x)) = x$. By using the leading, asymptotically free form, for $\alpha(\frac{s_I \rho}{\rho_{\text{peak}}^2}) \rho \stackrel{\text{large}}{\approx} \frac{2\pi}{\beta_0 \log(\frac{s_I \rho}{\rho_{\text{peak}}^2 \Lambda})} + \dots$, the inversion symmetry (11) then analytically leads again to a Cornell form

$$\alpha_s\left(\frac{s_I}{\rho}\right) \rho \stackrel{\text{large}}{\approx} -\frac{\pi}{N_c W\left(\frac{11}{6} \left(\frac{\rho_{\text{peak}}}{\rho}\right)^2 \ln\left(\frac{\rho_{\text{peak}}}{\rho}\right)\right)} \approx \frac{2\pi}{\beta_0} \frac{1}{\ln\left(\frac{\rho}{\rho_{\text{peak}}}\right)} \left(\frac{\rho}{\rho_{\text{peak}}}\right)^2 + \mathcal{O}(1), \quad (19)$$

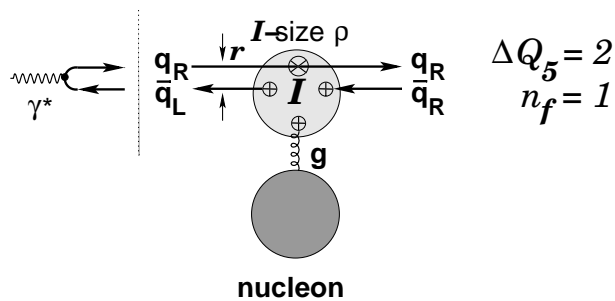


Figure 7. Illustration of the one-instanton contribution to the color-dipole picture[17] for the simplest instanton-induced process with $n_f = 1$ and no final-state gluons[5].

signalling confinement. More specifically, one may write down a simple and *exact* closed solution of Equation (18), ($\beta_0 = \frac{11}{3} N_c$),

$$\alpha_s\left(\frac{s_I}{\rho}\right) = \frac{2\pi}{\beta_0} \frac{\left(1 - \left(\frac{\rho}{\rho_{\text{peak}}}\right)^2\right)}{\ln\left(\frac{\rho_{\text{peak}}}{\rho}\right)}, \quad \text{with } \rho_{\text{peak}} = \frac{s_I}{\Lambda}, \quad (20)$$

which apparently now has “inherited” the inversion symmetry (11),

$$\left(\frac{\rho}{\rho_{\text{peak}}}\right) \alpha_s\left(\Lambda \frac{\rho}{\rho_{\text{peak}}}\right) = \left(\frac{\rho_{\text{peak}}}{\rho}\right) \alpha_s\left(\Lambda \frac{\rho_{\text{peak}}}{\rho}\right), \quad (21)$$

has *no Landau pole*, the correct asymptotic freedom form for $\rho \Rightarrow 0$ as well as a Cornell form (19) for large ρ . Amazingly, this (1-loop) form (20) of α_s exists already in the literature[28], but originated from an entirely different reasoning. It appeared as the appropriate (1-loop) running coupling without a Landau pole in sort of a renormalization-group improved variant of Shirkov’s “analytic perturbation theory” [29].

3.2. Instanton contribution to the color-dipole picture

Larger-size instantons may well play an important rôle in high-energy scattering processes[30] and even be the driving configurations for diffractive scattering[31], i. e. the (soft) \mathbb{P} omeron. As a well-defined start towards these important, but complicated issues, let us consider (initially at least) the DIS regime where I -perturbation theory holds. In this region, we then have recast[16] our published calculation of the simplest relevant I -induced process[5], $\gamma^* g \xrightarrow{(I)} q_R \bar{q}_R$, with one massless quark flavour into the language of the popular color-dipole picture[17] (c. f. Figure 7). The intuitive content of the latter is that at high energies, in the proton’s rest frame, the virtual photon fluctuates predominantly into a $q\bar{q}$ dipole a long distance upstream of the target proton. The large difference of the $q\bar{q}$ -formation and $(q\bar{q})$ - P interaction times then generically gives rise to the familiar factorized expression of the inclusive photon-proton cross sections

$$\sigma_{\gamma^* P}^{\text{LT}} = \int dz d^2\vec{r} |\Psi_{\gamma}^{\text{LT}}|^2 \sigma_{\text{dipole}}. \quad (22)$$

in terms of the modulus squared of the photon's (light-cone) wavefunction Ψ_γ^{LT} and the $(q\bar{q})$ - P dipole cross section σ_{dipole} . The important variables in Equation (22) are the transverse $(q\bar{q})$ -size \vec{r} and the photon momentum fraction z carried by the quark.

This dipole picture represents a convenient framework for discussing the transition from hard to soft physics (diffraction), with expectations

$$\begin{aligned} \text{“hard” (pQCD)[32]} & : \quad \text{small } \vec{r}^2 \sim \frac{1}{Q^2}, \quad \sigma_{\text{dipole}} = \alpha_s \mathcal{O}(\vec{r}^2), \quad \text{“color transparency”} \\ \text{“soft”} & : \quad \sqrt{\vec{r}^2} \gtrsim 0.5 \text{ fm}, \quad \sigma_{\text{dipole}} \approx \text{constant}, \quad \text{“hadron-like”}. \end{aligned} \quad (23)$$

In the large Q^2 regime, where I -perturbation holds, the I -contribution (Figure 7) may indeed be cast approximately into a form (22) and be compared to the familiar pQCD expression[32] (23). For reasons of space, let us just emphasize an emerging, striking feature: Unlike the pQCD expression[32] for σ_{dipole} , the required integrations over the I (\bar{I})-sizes now bring unavoidably as further length scale the effective (I -size)², $\langle \rho\bar{\rho}(Q^2, z) \rangle \propto \int \int d\rho d\bar{\rho} \rho^5 D(\rho) \bar{\rho}^5 D(\bar{\rho}) \{ \dots \}$, into the nominator that competes on dimensional grounds with the square of the transverse $(q\bar{q})$ -size \vec{r}^2 for $\vec{r}^2 \Rightarrow 0$. Since for a range of moderately high Q^2 , the effective I -size is dominated, however, by the peak-position $\rho_{\text{peak}} \approx 0.6$ fm of $\rho^5 dn/d^4x d\rho$ (c.f. Figure 6), the instanton in the background of the $(q\bar{q})$ -pair acts rather like an object of *hadronic* size and a roughly constant I -induced dipole cross section results,

$$\sigma_{\text{dipole}}^{(I)} \propto \frac{1}{\alpha_s} \langle \rho^2 \rangle \approx \text{constant}, \quad (24)$$

even for quite small $(q\bar{q})$ -size \vec{r}^2 . A detailed analysis of the delicate interplay of these two crucial length scales may be found in Ref. [16]. Thus, it seems that due to this precocious lack of “color transparency”, indeed, instanton configurations may well play a distinguished rôle in building up diffractive high-energy scattering.

Acknowledgements

All results on “small instantons and deep-inelastic scattering” (Section 2) have been obtained in long-term collaboration with Andreas Ringwald. Furthermore, I owe much insight about larger-size instantons to many discussions with Hans Joos.

- [1] Belavin A *et al.* 1975 *Phys. Lett.* **B59** 85
- [2] ‘t Hooft G 1976 *Phys. Rev. Lett.* **37** 8; 1976 *Phys. Rev.* **D14** 3432; 1978 *Phys. Rev.* **D18** 2199 (Erratum); 1986 *Phys. Rep.* **142** 357
- [3] Ringwald A and Schrempp F 1994 *Proc. Quarks '94*, ed D Yu Grigoriev *et al.* (Singapore: World Scientific) p 170
- [4] Balitsky I and Braun V 1993 *Phys. Lett.* **B314** 237
- [5] Moch S, Ringwald A and Schrempp F 1997 *Nucl. Phys.* **B507** 134
- [6] Ringwald A and Schrempp F 1998 *Phys. Lett.* **B438** 217
- [7] Ringwald A and Schrempp F 1999 *Phys. Lett.* **B459** 249
- [8] Carli T, Gerigk J, Ringwald A and Schrempp F 1999 *Proc. Monte Carlo Generators for HERA Physics (DESY-PROC-1999-02)* ed A T Doyle *et al.* (Hamburg: DESY) p 329
- [9] Ringwald A and Schrempp F 2000 *Comput. Phys. Commun.* **132** 267

- [10] Ringwald A and Schrempp F 2001 *Phys. Lett.* **B503** 331
- [11] Smith D A and Teper M J (UKQCD Collab.) 1998 *Phys. Rev.* **D58** 014505
- [12] Mikocki S (for the H1 Collaboration) 2000 *Proc. DIS 2000 (Liverpool)* ed J A Gracey and T Greenshaw (Singapore: World Scientific) p 322
- [13] H1 collaboration 2000 contr. paper to *30th Int. Conf. on High Energy Physics, ICHEP 2000 (Osaka)* <http://www-h1.desy.de/psfiles/confpap/ICHEP2000/H1prelim-00-025.ps>
- [14] Koblitz B (for the H1 Collaboration) 2001, talk at this meeting
- [15] Schrempp F 2001 to be published
- [16] Schrempp F and Utermann A 2001 to be published
- [17] Nikolaev N and Zakharov B G 1990 *Z. Phys.* **C49** 607; 1992 *Z. Phys.* **C53** 331; Mueller A H 1994 *Nucl. Phys.* **B415** 373
- [18] Bernard C 1979 *Phys. Rev.* **D19** 3013
- [19] Khoze V V and Ringwald A 1991 *Phys. Lett.* **B259** 106
- [20] Verbaarschot J 1991 *Nucl. Phys.* **B362** 33
- [21] Capitani S, Lüscher M, Sommer R and Wittig H 1999 *Nucl. Phys.* **B544** 669
- [22] Lönnblad L 1994 *Comput. Phys. Commun.* **71** 15
- [23] Jung H 1995 *Comput. Phys. Commun.* **86** 147
- [24] Caso C *et al.* (Particle Data Group) 1998 *Eur. Phys. J.* **C3** 1
- [25] Jackiw R and Rebbi C 1976 *Phys. Rev.* **D14** 517; Jackiw R, Nohl C and Rebbi C 1977 *Phys. Rev.* **D15** 1642
- [26] Crewther R 1972 *Phys. Rev. Lett.* **28** 1421; Chanowitz M and Ellis J 1972 *Phys. Lett.* **40B** 397; Collins J, Duncan A and Joglekar S 1977 *Phys. Rev.* **D16** 438
- [27] Yoneya T 1977 *Phys. Lett.* **71B** 407; Frolov I V and Schwarz A S 1979 *Phys. Lett.* **80B** 406; Corrigan E *et al.* 1979 *Nucl. Phys.* **B159** 469
- [28] Nesterenko A V 2000 *Mod. Phys. Lett.* **15** 2401
- [29] see e. g. Shirkov D V 2001 *Theor. Math. Phys.* **127** 409 and references therein
- [30] Shuryak E and Zahed I 2000 *Phys. Rev.* **D62** 085014
- [31] Kharzeev D E, Kovchegov Y V and Levin E 2001 *Nucl. Phys.* **A690** 621
- [32] Frankfurt L, Radyushkin A and Strikman M 1997 *Phys. Rev.* **D55** 98